Type I burst excitability

Carlo R. Laing*, Brent Doiron and André Longtin
Department of Physics, University of Ottawa, Ottawa, Canada K1N 6N5

Liza Noonan and Ray W. Turner
Department of Cell Biology and Anatomy, University of Calgary, Calgary, Canada T2N 4N1

Leonard Maler
Department of Cellular and Molecular Medicine, University of Ottawa, Ottawa, Canada K1H 8M5

* Corresponding author.
Institute of Information and Math Sciences, Massey University, Auckland, New Zealand.
Email: c.r.laing@massey.ac.nz
Ph: +64-9-443-9799 extn 9567. Fax: +64-9-441-8181

Keywords: bursting, excitable systems, pyramidal cells, electric fish, bifurcation.

Type I burst excitability

Carlo R. Laing (claing@science.uottawa.ca) †, Brent Doiron and André Longtin
Department of Physics, University of Ottawa, Ottawa, Canada K1N 6N5

Liza Noonan and Ray W. Turner
Department of Cell Biology and Anatomy, University of Calgary, Calgary, Canada T2N 4N1

Leonard Maler
Department of Cellular and Molecular Medicine, University of Ottawa, Ottawa, Canada K1H 8M5

November 12, 2002

Abstract. We introduce the concept of "type I burst excitability", which is a generalization of the "normal" excitability that is well–known in cardiac and neural systems. We demonstrate this type of burst excitability in a specific model system, a pyramidal cell from the electrosensory lateral line lobe of the weakly electric fish *Apteronotus leptorhynchus*. As depolarizing current is increased, a saddle–node bifurcation of periodic orbits occurs, which separates tonic and burst activity. This bifurcation is responsible for the excitable nature of the system, and is the basis for the "type I" designation. We verify the existence of this transition from *in vitro* recordings of a number of actual pyramidal cells. A scaling relationship between the magnitude and duration of a current pulse required to induce a burst is derived. We also observe this type of burst excitability and the scaling relationships in a multicompartmental model that is driven by realistic stochastic synaptic inputs mimicking sensory input. We conclude by discussing the relevance of burst excitability to communication between weakly electric fish.

1. Introduction

Bursting, in which a cell periodically switches from quiescent behavior to a rapidly spiking state and back again, is an important and common form of electrical activity (de Vreis, 1998; Izhikevich, 2000; Keener and Sneyd, 1998; Rinzel and Ermentrout, 1998). In this paper we introduce a specific example of what we term "burst excitability". Burst excitability is analogous to the "normal" excitability seen in neural, cardiac and other systems (Bub et al., 2002; Ermentrout, 1996; Glass and Mackey, 1988; Goldbeter, 1996; Izhikevich, 2000; Keener and Sneyd, 1998; Rinzel and Ermentrout, 1998), where a small, transient change in the input to a system causes it to undergo a large, stereotypical excursion in phase space before returning to its rest state. In neural systems, this large excursion corresponds to an action potential, while in cardiac systems it is a heart beat. In burst excitability, the large excursion in phase space is what would normally be classified as a "burst" in the bursting system, and the "rest state" that the system returns to may be periodic firing, as opposed to a true fixed point. Normal excitability often appears in systems that are close in parameter space to a saddle–node bifurcation of fixed points (Guckenheimer and Holmes, 1990; Kuznetsov, 1995), and which also have a "global connection" which the system approximately follows during the large excursion in phase space (Ermentrout, 1996; Gutkin and Ermentrout, 1998).

† Corresponding author.

We discuss burst excitability in a system which also has a saddle–node bifurcation, although of periodic orbits rather than fixed points, and which also has a "global connection" in phase space. Specifically, we discuss the "ghostburster" model of Doiron et al. (2002), a model of a pyramidal cell from the electrosensory lateral line lobe (ELL) of a weakly electric fish that is capable of burst discharge (Lemon and Turner, 2000). Previous work on a low–dimensional ODE model for this pyramidal cell showed that the transition from periodic to bursting behavior as the injected current was increased was a saddle–node bifurcation of periodic orbits (Doiron et al., 2002), and it is the presence of this bifurcation that provides a necessary ingredient for burst excitability. We refer to the type of burst excitability investigated here as "type I" in analogy with "normal" type I excitability, which involves a saddle–node bifurcation of fixed points (Ermentrout, 1996; Gutkin and Ermentrout, 1998).

In section 2 we briefly review "normal" excitability. In section 3 we introduce the pyramidal cell model that shows type I burst excitability, and in section 4 we discuss the saddle–node bifurcation of periodic orbits and show experimental data verifying the existence of a qualitative change from tonic to bursting behavior in ELL pyramidal cells as injected current is increased. In section 5 we demonstrate type I burst excitability in both the ghostburster model and a large multicompartment model (Doiron et al., 2001a). Section 6 contains an analysis of some of the properties of excitability, as derived from the normal form of the saddle–node bifurcation, and numerical verification of these results for both the low–dimensional pyramidal cell model we are studying and the multicompartment model of Doiron et al. (2001a). Finally we conclude in section 7 with a discussion of our results, in particular, with respect to coding of communication signals between fish.

2. "Normal" excitability

Excitability is a well–known phenomenon, observed in neural, cardiac and other systems. The usual notion of excitability is that a system is at rest and there exists a threshold such that if a perturbation pushes the system over threshold, it undergoes a large, stereotypical excursion in phase space (corresponding to e.g. the production of an action potential in a spiking neuron) before returning to rest. If the perturbation fails to push the system over threshold, the variables return directly to their resting values.

An example is shown in Figure 1, where we investigate the Morris–Lecar system (Keener and Sneyd, 1998; Rinzel and Ermentrout, 1998). Here we increase the input current I for a short amount of time before reducing it to its original value and observe the response of the system (see Appendix A for the equations describing this system, and Figure 2 of Gutkin and Ermentrout (1998) for a similar result). If the increase in current is not large enough (top panels) the system returns directly to its original fixed point (small closed loop in the top right panel). However, if the increase is sufficiently large (bottom panels) the system makes a large excursion in phase space before returning to rest. (Note that the trajectory that leaves the right side of the bottom right panel in Figure 1 returns through the left side and approaches the stable fixed point "A" from the left.) Most of

the large excursion in phase space occurs after I has been returned to its original value; the temporary increase in I was only necessary to push the system across the threshold — once across, the system must trace out a large excursion before returning to rest.

This form of excitability results from the fact that the bifurcation from quiescence to periodic firing as the input current is increased is a saddle–node bifurcation of fixed points (A and B), and that the two fixed points involved in the bifurcation lie on a topological circle, so that after they have annihilated one another a periodic orbit exists (Ermentrout, 1996; Gutkin and Ermentrout, 1998). The stable manifold of the saddle fixed point (B) acts as the threshold in this situation, and once this is crossed, a trajectory must closely follow part of the unstable manifold of this fixed point (which makes up part of the topological circle), making the large excursion in phase space before returning to the stable fixed point (A). It was this type of geometry that was used in the derivation of the "theta neuron" (Ermentrout, 1996; Gutkin and Ermentrout, 1998), a canonical model for this type of excitability.

This type of bifurcation to periodic firing as current is increased leads to "type I" neural dynamics, characterized by arbitrarily low firing frequencies as the current is varied. This is in contrast to "type II" dynamics, where the onset of periodic firing occurs at non–zero frequency, often through a Hopf bifurcation (Gutkin and Ermentrout, 1998; Rinzel and Ermentrout, 1998).

It should be noted that the large excursion in phase space before returning to a fixed point can involve the production of more than one action potential, a situation that Izhikevich (2000) called "burst excitability", and Av-Ron et al. (1993) referred to as "conditional bursting". However, neither of these papers contain any analysis of this phenomenon and both only mention the phenomenon in passing. Butera et al. (1995) studied the effects of transient current inputs to both real and model R15 bursting neurons that were either bathed in serotonin or dopamine, or had constant hyperpolarizing or depolarizing currents injected. They found behavior that we would call "burst excitability", but their analysis involved "quasi–steady–state I–V plots", rather than the geometric ideas that we use. A subsequent paper (Butera et al., 1997) did take a geometric approach, and the results presented here use similar ideas to those presented there. One significant difference, however, is that the underlying burst mechanisms are quite different.

3. The ghostburster model

We now present the ODE model of a pyramidal cell from the electrosensory lateral line lobe (ELL) of the weakly electric fish *Apteronotus leptorhynchus*. These fish sense weak electric fields due to either objects in their environment or their own nearly–periodic electric organ discharge (EOD) (Assad et al., 1999). The electric field is sensed by electroreceptors that cover the fish's body (see e.g. Nelson et al. (1997) and references therein). In general, these electroreceptors produce more action potentials as the amplitude of the electric field at the surface of the fish's skin is increased (Xu et al., 1996). They make both excitatory

and inhibitory (through an interneuron) connections to a layer of pyramidal cells in the ELL (Berman and Maler, 1999).

The pyramidal cell model, previously discussed in Doiron et al. (2002), was a reduction of a multicompartmental model presented in Doiron et al. (2001a). The reduction was achieved by lumping the many compartments into two, representing the soma and the dendrite of the cell, and by ignoring the dynamics of channels not thought to be important for the bursting behavior.

The model consists of two isopotential compartments, representing the soma and dendrite of the neuron. They are diffusively coupled through voltage, following (among others) Mainen and Sejnowski (1996) and Pinsky and Rinzel (1994). The equations governing the system, previously presented in (Doiron et al., 2002), are:

$$\begin{aligned} C\frac{dV_s}{dt} &= I - g_{Na,s}[m_{\infty,s}(V_s)]^2(h_0 - n_s)(V_s - V_{Na}) - g_{dr,s}n_s^2(V_s - V_K) \\ &\quad -g_L(V_s - V_L) - \frac{g_c}{\kappa}(V_s - V_d) \qquad (1) \\ \frac{dn_s}{dt} &= \frac{n_{\infty,s}(V_s) - n_s}{0.39} \qquad (2) \\ C\frac{dV_d}{dt} &= -g_{Na,d}[m_{\infty,d}(V_d)]^2 h_d(V_d - V_{Na}) - g_{dr,d}n_d^2 p_d(V_d - V_K) \\ &\quad -g_L(V_d - V_L) - \frac{g_c}{1-\kappa}(V_d - V_s) \qquad (3) \\ \frac{dh_d}{dt} &= h_{\infty,d}(V_d) - h_d \qquad (4) \\ \frac{dn_d}{dt} &= \frac{n_{\infty,d}(V_d) - n_d}{0.9} \qquad (5) \\ \frac{dp_d}{dt} &= \frac{p_{\infty,d}(V_d) - p_d}{5} \qquad (6) \end{aligned}$$

Subscripts s and d refer to somatic and dendritic variables, respectively. The variables m and h are activation and inactivation of Na^+, respectively, and n and p are activation and inactivation of K^+, respectively. Parameter values are $C = 1$, $g_{Na,s} = 55$, $h_0 = 1$, $V_{Na} = 40$, $g_{dr,s} = 20$, $V_K = -88.5$, $g_L = 0.18$, $V_L = -70$, $g_c = 1$, $\kappa = 0.4$, $g_{Na,d} = 5$, $g_{dr,d} = 15$. I is the somatic input current, g_c is the coupling conductance, and κ is the ratio of the somatic area to the total area of the cell. Other functions are $m_{\infty,s}(V) = 1/[1 + \exp(-(V + 40)/3)]$, $n_{\infty,s}(V) = 1/[1 + \exp(-(V + 40)/3)]$, $m_{\infty,d}(V) = 1/[1 + \exp(-(V + 40)/5)]$, $h_{\infty,d}(V) = 1/[1 + \exp((V + 52)/5)]$, $n_{\infty,d}(V) = 1/[1 + \exp(-(V + 40)/5)]$, $p_{\infty,d}(V) = 1/[1 + \exp((V + 65)/6)]$. For details and derivation of these equations, see Doiron et al. (2001a) and Doiron et al. (2002).

This model reproduced burst discharge qualitatively similar to that seen in experiments (Lemon and Turner, 2000; Turner and Maler, 1999). During bursting, the behavior of the system is as follows (Lemon and Turner, 2000). After most somatic action potentials, a dendritic action potential occurs. Experimental recordings show that the half–width of a dendritic action potential is larger than the half–width of the corresponding somatic one (Lemon and Turner, 2000), and this is incorporated into the model through different time–constants for the somatic versus dendritic channels. Because of this difference in half–

widths, current flows from the dendrite to the soma immediately after the somatic action potential, causing a depolarizing afterpotential (DAP) at the soma. This DAP decreases the amount of time until the next somatic action potential. Because of the slow time–scale of inactivation of dendritic potassium (the variable p_d in (6)) the sizes of these DAPs slowly increase, leading to successively shorter interspike intervals (ISIs). This continues until a somatic ISI is smaller than the refractory period of the dendrite and the dendrite fails to produce an action potential in response to a somatic one, so little current flows from the dendrite to the soma, no DAP appears, and the next ISI is long. The process then repeats. These long ISIs, each of which immediately follows a very short one, divide a train of action potentials into bursts. Figure 2 shows a typical series of bursts from the model (1)-(6). A detailed description of this burst mechanism is presented in Lemon and Turner (2000) and Doiron et al. (2001a).

If the current injected into the soma is decreased, there is enough time between action potentials for the variable controlling dendritic inactivation of potassium (p_d) to recover fully. Thus successive DAPs do not grow in size and the neuron fires periodically. An example is shown in Figure 3, where the somatic voltage as a function of time is shown for 4 different values of injected current. The qualitative difference in behaviors for low and high I imply that there must be a bifurcation separating periodic from burst firing as I is increased.

4. Saddle–node bifurcation

4.1. Model results

It was found in Doiron et al. (2002) that if the current to the soma (I) is gradually increased, the system (1)-(6) switches from quiescence (a fixed point) to periodic firing and then to bursting, in contrast with many other bursting systems (Pinsky and Rinzel, 1994; Steriade et al., 1998; Terman, 1992). The transition from periodic firing to bursting behavior was found to be caused by a saddle–node bifurcation of periodic orbits (Kuznetsov, 1995). These orbits and the bifurcation are shown in Figure 4, a bifurcation diagram for (1)-(6) as a function of I. (See also Figure 3.) For smaller values of I, a stable and an unstable periodic orbit coexist. As I is increased they annihilate one another and the system behaves in a complex, chaotic fashion (Doiron et al., 2002). This bifurcation is necessary for this type of burst excitability, as will be seen.

4.2. Experimental Results

The existence of the transition from periodic to bursting behavior as I is varied is also seen in data from actual pyramidal cells. Sharp electrode intracellular recordings were obtained from ELL pyramidal cells for which a constant depolarization, I, was applied for 4 seconds. To show the transition as a function of injected current we use a quantity (previously introduced in Doiron et al. (2001b)) that will enable us to distinguish between

voltage records that show mostly periodic behavior and records that show mostly bursting. For each somatic voltage train, we find the minimum voltage between each pair of action potentials and label these ν_i for $i = 1, \ldots, N$, where there are N such minima in the particular trace being examined. We then form the average of the square of the differences between successive pairs of ν_i, defining

$$\Sigma \equiv \frac{1}{N-1} \sum_{i=2}^{N} (\nu_i - \nu_{i-1})^2 \tag{7}$$

For periodic firing, $\nu_i = \nu_{i-1}$ for $2 \leq i \leq N$, so Σ will equal zero for this case. During bursting, there is a gradual increase in the values of ν_i during a burst and then a sudden drop during the long interburst interval (see Figure 2, top panel, and Figure 3). Thus each pair, $\nu_i - \nu_{i-1}$, will be nonzero and contribute to the sum. Since it is mainly the interburst intervals that contribute to the sum, and the number of action potentials per burst decreases as I is increased above the bifurcation value (Doiron et al., 2002), Σ will increase as I increases past the bifurcation value (~ 8.5, from Figure 4).

In Figure 5 we show Σ for both experimental and model data. The top and middle panels of Figure 5 show Σ, defined in (7), as a function of somatic input current for two different pyramidal cells during recordings of duration four seconds, and the bottom panel shows the same quantity for the model (1)-(6). Data from six other cells was recorded and shows similar behavior to that in the top two panels (data not shown). A number of other cells were recorded from but did not show bursting for the range of currents tested, which is in agreement with previous studies (Lemon and Turner, 2000). There was a large variability in the maximum value of Σ and the value of I at which the transition occurred. This is to be expected, due to the known variability in dendritic arborization (Bastian and Courtright, 1991; Bastian and Nguyenkim, 2001). This variability affects the threshold for bursting and the range of possible spiking patterns, among other properties (Laing et al., 2002).

The existence of current values at which both the actual and model cells switch from periodic to bursting behavior is clear. The experimental data presented here and in Lemon and Turner (2000) strongly suggests that the actual cells undergo a saddle–node bifurcation of periodic orbits as the current injected to the soma is varied. Furthermore, the average burst length in data from these cells has been observed to scale as the inverse of the square root of the amount by which the current is superthreshold (Doiron et al., 2001b). This saddle–node bifurcation of periodic orbits is a necessary ingredient for type I burst excitability.

5. Burst Excitability

Since the bifurcation terminating periodic firing as I is increased in the system (1)-(6) (see Figure 4) is a saddle–node bifurcation of periodic orbits (Doiron et al., 2002), in analogy with normal type I excitability we have the possibility of excitable behavior. The other necessary ingredient is a "global reinjection" mechanism, analogous to the topological circle

mentioned in section 2, which, after the periodic orbits have been annihilated, provides a mechanism for a large excursion in phase space and return to a periodic orbit. We do have this "reinjection", as can be seen in the behavior of p_d during a burst (Figure 2, bottom panel). The variable p_d gradually decreases through a burst, but cannot continue to do this forever, as eventually the effect of the dendritic refractory period come into play, the burst terminates, and p_d rapidly increases — this is the reinjection.

(For the study of burst excitability in the ghostburster, we are making an analogy between the saddle–node bifurcation of fixed points in the Morris–Lecar system (Figure 1) and the saddle–node bifurcation of periodic orbits in the ghostburster. However, for burst excitability in other bursting systems, other bifurcations may relevant.)

For a value of I just below that corresponding to the periodic to bursting transition, the stable manifold of the unstable periodic orbit acts as a threshold — if this is crossed, p_d starts to decrease and continues to do so until the burst terminates and the trajectory returns to the stable periodic orbit. An example of this is shown in Figure 6. At a current of 8.3, the neuron fires periodically. The current is stepped from 8.3 to either 10.5 or 11 for 10 ms, and then returned to 8.3. The step to 10.5 fails to induce a burst and the variables return directly to their previous (periodic) values, but a step to 11 pushes the system over threshold, p_d decreases until the end of the burst, and then the variables return to their previous values. Note that most of the burst occurs after I has been returned to 8.3, another signature of the excitable nature of the system.

Thus, for the system (1)-(6), we have a new form of excitability, analogous to the usual form with the associations

Normal excitability	Type I burst excitability
fixed point	periodic firing
action potential	burst

However, the analogy is not exact since before the perturbation the system (1)-(6) is periodically oscillating, rather than at a fixed point, and the phase of the oscillation at which the perturbation is applied must be taken into consideration. The value of this phase can greatly affect the resulting burst. This is demonstrated in Figure 7, where two identical current pulses are applied but at slightly different phases of the underlying oscillation (the actual difference in phases for the two situations is approximately 1/8 of a cycle). Note that the time between the onset of the pulse and the termination of the burst is very different in the two cases. Another difference, also related to the more complex nature of the underlying system, is that the bursts are not highly stereotyped. They all terminate in a high frequency "doublet", but as mentioned, the number of action potentials between the stimulus onset and the doublet is highly variable.

The duration of the applied current steps is compatible with the synaptic input to the pyramidal cell resulting from the detection of a "chirp", a transient modulation of both the frequency and amplitude of a fish's EOD. Zupanc and Maler (1993) found that chirps could be evoked in *Apteronotus leptorhynchus* by imitating the EOD of a neighboring fish, and proposed that chirps are involved in communication between fish. They found that

chirps typically last about 15 ms and involve an increase in the frequency of the chirping fish of about 100 Hz. Chirps produce transient increases in excitatory synaptic input to pyramidal cells (unpublished observations) that result in the production of a small number of spikes (Metzner and Heiligenberg, 1991). This provides motivation for the form of the current pulses used in Figures 6 and 7.

To demonstrate type I burst excitability in these pyramidal cells in a more realistic manner, we have simulated a transient input to a realistic multicompartmental model of a pyramidal cell *in vivo*. The model used was presented in Doiron et al. (2001a). The cell has both proximal and apical dendritic compartments, constructed from a digitized image of a Lucifer yellow stained basilar pyramidal cell; the apical compartments contain channels responsible for the active backpropagation necessary for bursting. A single basilar dendrite extends from the soma for approximately 200 μm, after which the dendrite branches to form a bush–like structure. The electroreceptor afferents synapse excitatorily to this bush.

Lateral segment pyramidal cells have been shown to be required for the detection of communication signals (chirps) (Metzner, 1999). To simulate one of these cells, we spread 1000 excitatory synapses over the basilar bush of the neuron — these model afferent connections. This number is estimated from data on receptive field sizes (Bastian et al., 2002) and receptor density (Carr et al., 1982). The synaptic events are modeled as currents of the form $-g(t)(V(t)-0)$, where $V(t)$ is the voltage of the compartment to which the synapse is attached (i.e. the reversal potential is 0) and $g(t)$ follows an alpha function

$$g(t) = \widehat{g}\left(\frac{t}{\tau}\right) e^{1-t/\tau} \tag{8}$$

after each firing time, where $\widehat{g} = 6$ pS and $\tau = 1.5$ msec (i.e. AMPA synapses). These parameters are appropriate for modeling afferent–evoked EPSPs in pyramidal cells (Berman and Maler, 1999). (The maximal conductance was chosen so as to produce realistic changes in the firing rate of the pyramidal cell, given the firing rates of the afferent inputs.) The synaptic firing times were chosen from independent Poisson distributions. The firing rate of each synapse was originally set at 150 Hz, and then stepped to either 475 or 400 Hz when $250 < t < 270$, i.e. for 20 msec. These values are consistent with the responses of electroreceptors during chirp stimuli (unpublished observations) (Metzner and Heiligenberg, 1991).

As can be seen in Figure 8, the step to 400 Hz did not induce a burst, but the step to 475 Hz did. The first and third panels of Figure 8 show the somatic voltage, and the second and fourth show the sum of the conductances from all 1000 synapses as a function of time (compare with Figure 6). Thus in a much more realistic model of the pyramidal cell, and with more realistic stochastic inputs, we also have type I burst excitability.

This form of burst excitability was also observed by Laing and Longtin (2002) in a reduced model of the system (1)-(6). The model presented there used an integrate–and–fire neuron to produce action potentials, and a second variable that mimicked the effects of the slowly changing dendritic potassium in (1)-(6).

6. Analysis

6.1. Theory

Both the normal and burst excitability that we have analyzed arise from saddle–node bifurcations — of fixed points in normal excitability and of periodic orbits in burst excitability. The normal form of this bifurcation can be used to derive the minimum pulse strength and duration needed to induce a burst (or action potential). We first examine normal excitability.

The normal form of the saddle–node bifurcation of fixed points in a continuous–time dynamical system is (Guckenheimer and Holmes, 1990; Kuznetsov, 1995)

$$\frac{dx}{dt} = \mu + x^2 \tag{9}$$

This governs the behavior on the center manifold. For $\mu < 0$ there are two fixed points, $x^{\pm} \equiv \pm\sqrt{-\mu}$. The point x^- is stable with basin of attraction $(-\infty, x^+)$, and x^+ is unstable. For $\mu > 0$ there are no fixed points. The current pulses discussed above for normal excitability correspond to switching μ from a negative value to a positive one for a short amount of time, and then back again. Assume for concreteness that before the pulse, $\mu = -\nu$, $(\nu > 0)$, and that during the pulse $\mu = \lambda$, $(\lambda > 0)$. For $\mu > 0$, the solution of (9) is

$$x(t) = \sqrt{\mu}\tan\left[\sqrt{\mu}t + \tan^{-1}\left(\frac{x(0)}{\sqrt{\mu}}\right)\right] \tag{10}$$

where $x(0)$ is the value of x at time 0. For a pulse of duration T to cause an action potential, we need $x(T) > x^+$, where $x(0) = x^-$, i.e. for x to escape the basin of attraction of the stable fixed point during the pulse, having started at the stable fixed point. Once x has escaped the basin of attraction it will make a large excursion and then return to the stable fixed point. (The normal form (9) is only a local description of the dynamics, and does not describe the large excursion.) The above inequality is equivalent to

$$\sqrt{\nu} < \sqrt{\lambda}\tan\left[\sqrt{\lambda}T + \tan^{-1}\left(\frac{-\sqrt{\nu}}{\sqrt{\lambda}}\right)\right] \tag{11}$$

which, under the assumption that $\sqrt{\nu/\lambda}$ is small so that $\tan x \approx \tan^{-1} x \approx x$, can be written

$$\frac{2\sqrt{\nu}}{\lambda} < T \tag{12}$$

Thus the minimum value of T that will induce an action potential scales as

$$T \sim \frac{\sqrt{\nu}}{\lambda} \tag{13}$$

The analysis of type I burst excitability is very similar, except that one should now study the normal form of the saddle–node bifurcation of fixed points in a map:

$$x_{n+1} = x_n + \mu + x_n^2 \tag{14}$$

where n is an integer. This map can be derived by placing a Poincaré section in the flow, reducing the study of a periodic orbit in a continuous–time system to the study of a fixed point of a discrete–time map (Guckenheimer and Holmes, 1990; Kuznetsov, 1995). For $\mu < 0$, the map (14) has two fixed points, $\pm\sqrt{-\mu}$, which are destroyed in a saddle–node bifurcation at $\mu = 0$ in the same way as for (9). A bifurcation of this form (which corresponds to a saddle–node bifurcation of periodic orbits in a flow) can be observed in (1)-(6) by placing a Poincaré section in the flow, as was shown in Doiron et al. (2002). The scaling relationship obtained from (14) is also given by (13).

6.2. Numerical results

In Figure 9 we show numerical results for the system (1)-(6) that are consistent with the scaling of (13). Here, the current before a pulse (effectively ν) is held constant while the height of the pulse (effectively λ) is increased. We measured the minimum duration of a pulse needed to produce a burst with probability 0.5. We have to take this probabilistic approach for burst excitability as the "rest state" is now periodic firing, and the time of the onset of the pulse relative to the phase of the periodic firing has to be considered (see Figure 7). (This would also be the case if, e.g. the system shown in Figure 1 was weakly periodically forced.)

To obtain Figure 9, a number of pulses were applied at random phases of the periodic oscillation. (The time between pulses was sufficient for the system to relax back to the periodic orbit.) The average number of bursts per pulse is a continuous function of both pulse duration and strength, and curves for probabilities other than 0.5 are similar to that shown in Figure 9. As predicted by (13), the minimum pulse duration required to induce a burst for a fixed baseline current (effectively ν) is inversely proportional to the height of the pulse above the value needed to produce bursting. (The offset, 0.1235, in the caption of Figure 9 is a result of the pulse height being $\nu + \lambda$, not just λ.) The baseline current was set at $I = 8.3$.

Note that a plot of the form shown in Figure 9 but with the axes interchanged (i.e. a plot of the stimulus intensity necessary to evoke a response as a function of stimulus duration) is often known as a "strength–duration curve". However, these are usually constructed for normal excitability, where the event is a single action potential rather than a burst of them.

Figure 10 is further confirmation that the relationship (13) holds for (1)-(6). Here the height of the pulse (effectively λ) is held constant while the current before the pulse (effectively ν) is varied. Note that ν increases as I decreases. As in Figure 9, we measure the minimum duration of a pulse needed to produce, on average, one burst for every two pulses applied. We see that this duration is proportional to the square root of the difference between the baseline current and the current needed to produce bursting (solid line), in agreement with (13). An even better fit can be obtained by keeping the full expression (11), which gives

$$T \sim \tan^{-1}(\alpha\sqrt{\nu}) \tag{15}$$

for some α, assuming that λ is fixed (dashed line in Figure 10).

The scaling results of (13) also hold for the multicompartment model of Doiron et al. (2001a), discussed in Section 5. Recall that we change the input strength by modulating the firing rate of the independent Poisson processes associated with each of the 1000 excitatory synapses. In Figure 11 we show a plot of the minimum duration of a pulse required to generate a burst as a function of the strength of the pulse. The firing rate prior to the pulse, and after it, was 150 Hz. We see that the simulation results are consistent with the theory.

In Figure 12 we show further confirmation that the scaling given (13) holds for the multicompartment model of Doiron et al. (2001a). We have kept the intensity of each pulse constant at 475 Hz, but varied the rate of synaptic activity before and after the pulse (they are the same) and determined how this affects the duration of a pulse required to produce one burst. We see that again the simulations agree well with the theory, particularly when the baseline activity is close to the threshold between tonic and bursting behavior (225 Hz, from Figure 12).

Note that while the numerically obtained results above are consistent with there being a saddle–node bifurcation of periodic orbits separating periodic from bursting behavior, other model neurons could have other bifurcations that separate these types of behavior and produce the same form of scaling.

7. Discussion and conclusion

We have introduced and analyzed the new phenomenon of type I burst excitability, presenting it in a specific system, a "ghostburster" pyramidal cell, and in a specific context, the detection of communicatory signals. Briefly, the existence of a saddle–node bifurcation of periodic orbits, together with a "global reinjection" through phase space, enable us to make an analogy with normal excitability:

Normal excitability	Type I burst excitability
fixed point	periodic firing
action potential	burst

The analogy is not exact, as the underlying phase of the periodic oscillation at the onset of the transient input must be taken into account, and the bursts are not as highly sterotyped as action potentials in normal excitability. We have shown data from actual pyramidal cells which strongly suggests that these cells possess the necessary ingredients for this type of burst excitability, and we have also simulated it in a realistic multicompartment model of a pyramidal cell driven by stochastic inputs. We have derived and verified a scaling law relating the strength and duration of the current pulses required to observe a superthreshold response of an excitable system.

The pyramidal cells studied are sensory neurons, receiving input directly from electroreceptors on the surface of the fish, and thus it is reasonable to assume that they process electrosensory information in some way and pass it to higher brain regions. As mentioned,

the type of input current required to induce a burst in these cells is compatible with the output of electroreceptors (unpublished observations) that detect a chirp from another fish (Zupanc and Maler, 1993).

The production of a burst by a pyramidal cell in the ELL in response to a sudden artificial increase in EOD amplitude has recently been seen *in vivo* (J. Bastian, personal communication). These bursts were observed by recording from the dendrite of a pyramidal cell, and both the decreasing ISIs during the burst and the sudden decrease in spike amplitude at the end of the burst indicate that this was the same type of burst as discussed here and elsewhere (Doiron et al., 2002; Doiron et al., 2001a; Lemon and Turner, 2000). These burst responses were suppressed by hyperpolarization of the cell, which is consistent with the existence of a threshold in current for burst behavior.

More generally, the current input to a ghostbursting cell will not be constant, but will have slow modulations. These could be due to objects passing close to the fish, or a result of the "beat" frequency that occurs when two fish with different EOD frequencies are close to one another. (The beat frequency is equal to the difference between the EOD frequencies of the two fish; recall that EODs are quasi–sinusoidal.) The results in Figure 7 show that the response of a pyramidal cell to identical inputs depends on the phase of the periodic firing of the cell, but it may also be the case that the response will be different during different parts of the cycle associated with the beating frequency. Indeed, Zupanc and Maler (1993) showed that the form of chirps emitted by male fish in response to a simulated EOD depended on the phase of the beat cycle created between the fish's own EOD and the simulated EOD, and any system for detecting such chirps may also take into account the phase of the beat cycle.

Lisman (1997) recently proposed that bursts, rather than individual action potentials, may be fundamental units of neural information. One reason behind this idea is that many synapses are unreliable, but due to facilitation a burst of action potentials may be signaled reliably in a situation where a single action potential may not. The system described in this paper may be an example for which this principle applies, since the burst terminates with a high–frequency "doublet" event. Simultaneous burst discharge by a number of pyramidal cells that synapse onto a common target cell would presumably be more reliable than a transient increase in the rate of asynchronous firing of those cells.

Other bursting systems also have bifurcations that separate periodic or quiescent behavior from bursting as input current is changed (Terman, 1992). We have simulated the square–wave, parabolic and elliptic bursters described in Rinzel and Ermentrout (1998), and found that these systems also have such bifurcations. These bursters all follow the pattern quiescence $\rightarrow$ bursting $\rightarrow$ tonic as current is increased (not shown), in contrast with the system (1)-(6). We have found that transient changes in input current across the bifurcation points separating these regimes also cause behavior that is qualitatively similar to that discussed above — a motion in phase space that would be labeled a burst if the system was bursting, followed by a return to either periodic or quiescent behavior, depending on the state of the system before the perturbation (results not shown). This is the behavior observed by Izhikevich (2000) and Av-Ron et al. (1993); their systems were close to the quiescent/bursting boundary. Butera et al. (1995) saw similar behavior

in model and real R15 neurons and in a subsequent paper analyzed the model in a way similar to that performed here (Butera et al., 1997). However, the bifurcations involved in the transitions from bursting to other types of behavior in these models are often very complicated (Terman, 1992), rather than simple saddle–node bifurcations. Also, the models described in Rinzel and Ermentrout (1998) are not models of sensory neurons, so it is harder to speculate about the "meaning" of burst excitability in such neurons. This is in contrast with the system (1)-(6), which represents a neuron thought to play an important role in sensory processing.

It should also be mentioned that there are other model neurons which are capable of bursting, but which do not follow the pattern quiescence $\rightarrow$ bursting $\rightarrow$ tonic as injected current is increased. An example is integrate–and–fire–or–burst model of a thalamocortical relay neuron (Smith et al., 2000), which moves from quiescence to a single burst to quiescence and finally to periodic firing as the injected DC current is gradually increased.

The simulations mentioned above, and the results of others (Av-Ron et al., 1993; Butera et al., 1995; Izhikevich, 2000), suggest that burst excitability is a general phenomenon in systems capable of bursting. We have analyzed the behavior of one particular type in a particular model, as did Butera et al. (1997); the analysis of other bursting systems under time–varying input remains to be done.

Acknowledgements: We acknowledge financial support from NSERC (B.D., L.N., A.L), OPREA (C.L., A.L.) and CIHR (A.L., R.T., L.M.). R.T. is an Alberta Heritage Senior Scholar. We thank the referees for bringing Butera et al. (1995) and Butera et al. (1997) to our attention.

References

Av-Ron, E., Parnas, H. and Segel, L. A. (1993). A basic biophysical model for bursting neurons. *Biol. Cybern.* **69**, 87-95.

Assad C., Rasnow, B. and Stoddard, P.K. (1999). Electric organ discharges and electric images during electrolocation *J. Exp. Biol.* **202**, 1185-1193.

Bastian, J., Chacron, M. J. and Maler, L. (2002). Receptive field organization determines pyramidal cell stimulus encoding capability and spatial stimulus selectivity. *J. Neurosci.*, **22**, 4577-4590.

Bastian, J. and Courtright, J. (1991). Morphological correlates of pyramidal cell adaptation rate in the electrosensory lateral line lobe of weakly electric fish. *J. Comp. Physiol. A*, **168**(4), 393-407.

Bastian, J. and Nguyenkim, J. (2001). Dendritic modulation of burst–like firing in sensory neurons. *J. Neurophysiol.* **85**, 10-22.

Berman, N. J. and Maler, L. (1999). Neural architecture of the electrosensory lateral line lobe: adaptations for coincidence detection, a sensory searchlight and frequency–dependent adaptive filtering. *J. Exp. Biol.* **202**, 1243-1253.

Bub, G., Shrier, A. and Glass, L. (2002). Spiral wave generation in heterogeneous excitable media. *Phys. Rev. Lett.* **88**, 058101.

Butera, R. J., Clark, J. W., Canavier, C. C., Baxter, D. A. and Byrne, J. H. (1995). Analysis of the effects of modulatory agents on a model bursting neuron: dynamic interactions between voltage and calcium dependent systems. *J. Comput. Neurosci.* **2**, 19-44.

Butera, R. B., Clark, J. W. and Byrne, J. H. (1997). Transient responses of a modeled bursting neuron: analysis with equilibrium and averaged nullclines. *Biol. Cyber.* **77**, 307-322.

Carr, C., Maler, L. and Sas, E. (1982). Peripheral organization and central projections of the electrosensory nerves in gymnotiform fish. *J. Comp. Neurol.* **211**, 139-153.

de Vreis, G. (1998). Multiple bifurcations in a polynomial model of bursting oscillations. *J. Nonlinear Sci.* **8** 281-316.

Doiron, B., Laing, C. R., Longtin, A. and Maler, L. (2002). "Ghostbursting": a novel bursting mechanism in pyramidal cells. *J. Comput. Neurosci.* **12**(1), 5-25.

Doiron, B., Longtin, A., Turner, R.W. and Maler, L. (2001a). Model of gamma frequency burst discharge generated by conditional backpropagation. *J. Neurophysiol.* **86**(4), 1523-1545.

Doiron, B., Noonan, L., Turner, R. W., Longtin, A., and Maler, L. (2001b). Shifting burst threshold with dendritic conductances. XXXI Proc. Soc. Neurosci., San Diego.

Ermentrout, G. B. (1996). Type I membranes, phase resetting curves, and synchrony. *Neural Comp.* **8** 979-1001.

Glass, L. and Mackey, M. C. (1988). *From clocks to chaos: the rhythms of life.* Princeton University Press.

Goldbeter, A. (1996). *Biochemical oscillations and cellular rhythms: the molecular bases of periodic and chaotic behaviour.* Cambridge University Press.

Guckenheimer, J. and Holmes, P. (1990). *Nonlinear oscillations, dynamical systems and bifurcations of vector fields.* Applied Mathematical Sciences, Vol. 42. Springer–Verlag.

Gutkin, B. S. and Ermentrout, G. B. (1998). Dynamics of membrane excitability determine inter–spike interval variability: a link between spike generation mechanisms and cortical spike train statistics. *Neural Comp.* **10** 1047-1065.

Izhikevich, E. M. (2000). Neural excitability, spiking, and bursting. *Int. J. Bifn. Chaos* **10** 1171-1266.

Keener, J. and Sneyd, J. (1998). *Mathematical Physiology.* Interdisciplinary Applied Mathematics, Vol. 8. Springer–Verlag New York.

Kuznetsov, Y. A. (1995). *Elements of Applied Bifurcation Theory.* Applied Mathematical Sciences, Vol. 112. Springer–Verlag.

Laing, C. R., Doiron, B., Longtin, A. and Maler, L. (2002). Ghostbursting: the effects of dendrites on spike patterns. *Neurocomputing,* **44-46** 127-132.

Laing, C. R. and Longtin, A. (2002). A two–variable model of somatic–dendritic interactions in a bursting neuron. *Bull. Math. Biol.*, **64** 829-860.

Lemon, N. and Turner, R. (2000). Conditional spike backpropagation generates burst discharge in a sensory neuron. *J Neurophysiol* **84** 1519-1530.

Lisman, J. E. (1997). Bursts as units of neural information: making unreliable synapses reliable. *Trends Neurosci* **20** 38-43.

Mainen, Z. F. and Sejnowski, T. J. (1996). Influence of dendritic structure on firing pattern in model neocortical neurons. *Nature* **382** 363-366.

Metzner, W. (1999). Neural circuitry for communication and jamming avoidance in gymnotiform electric fish *J. Exp. Biol.* **202**, 1365-1375.

Metzner, W. and Heiligenberg, W. (1991). The coding of signals in the electric communication of the gymnotiform fish Eigenmannia: from electroreceptors to neurons in the torus semicircularis of the midbrain. *J. Comp. Physiol. [A],* **169**, 135-150.

Nelson, M. E., Z. Xu and J. R. Payne (1997). Characterization and modeling of P–type electrosensory afferent responses to amplitude modulations in a wave–type electric fish. *J. Comp. Physiol. A* **181** 532-544.

Pinsky, P. F. and Rinzel, J. (1994). Intrinsic and network rhythmogenesis in a reduced Traub model for CA3 neurons. *J. Comput. Neurosci.* **1** 39-60.

Rinzel, J. and Ermentrout, G. B. (1998). Analysis of neural excitability and oscillations. In *Methods in Neuronal Modeling: From Ions to Networks.* Ed. Koch, C. and Segev, I. MIT Press.

Smith, G. D., Cox, C. L., Sherman, S. M. and Rinzel, J. (2000). Fourier analysis of sinusoidally driven thalamocortical relay neurons and a minimal integrate–and–fire–or–burst model. *J. Neurophysiol.* **83** 588-610.

Steriade, M., I. Timofeev, N. Dürmüller and F. Grenie (1998). Dynamic properties of corticothalamic neurons and local cortical interneurons generating fast rhythmic (30-40 Hz) spike bursts. *J. Neurophysiol.* **79** 483-490.

Terman, D. (1992). The transition from bursting to continuous spiking in excitable membrane models. *J. Nonlinear Sci.* **2**(2), 135-182.

Turner, R. W. and Maler, L. (1999). Oscillatory and burst discharge in the Apteronotid electrosensory lateral line lobe. *J. Exp. Biol.* **202** 1255-1265.

Xu, Z., Payne, J.R. and Nelson, M.E. (1996) Logarithmic time course of sensory adaptation in electrosensory afferent nerve fibers in a weakly electric fish. *J. Neurophysiol.* **76**, 2020-2032.

Zupanc, G. K. H. and Maler, L. (1993). Evoked chirping in the weakly electric fish (Apteronotus leptorhynchus): a quantitative biophysical analysis. *Can. J. Zool.* **71**, 2301-2310.

List of Figures

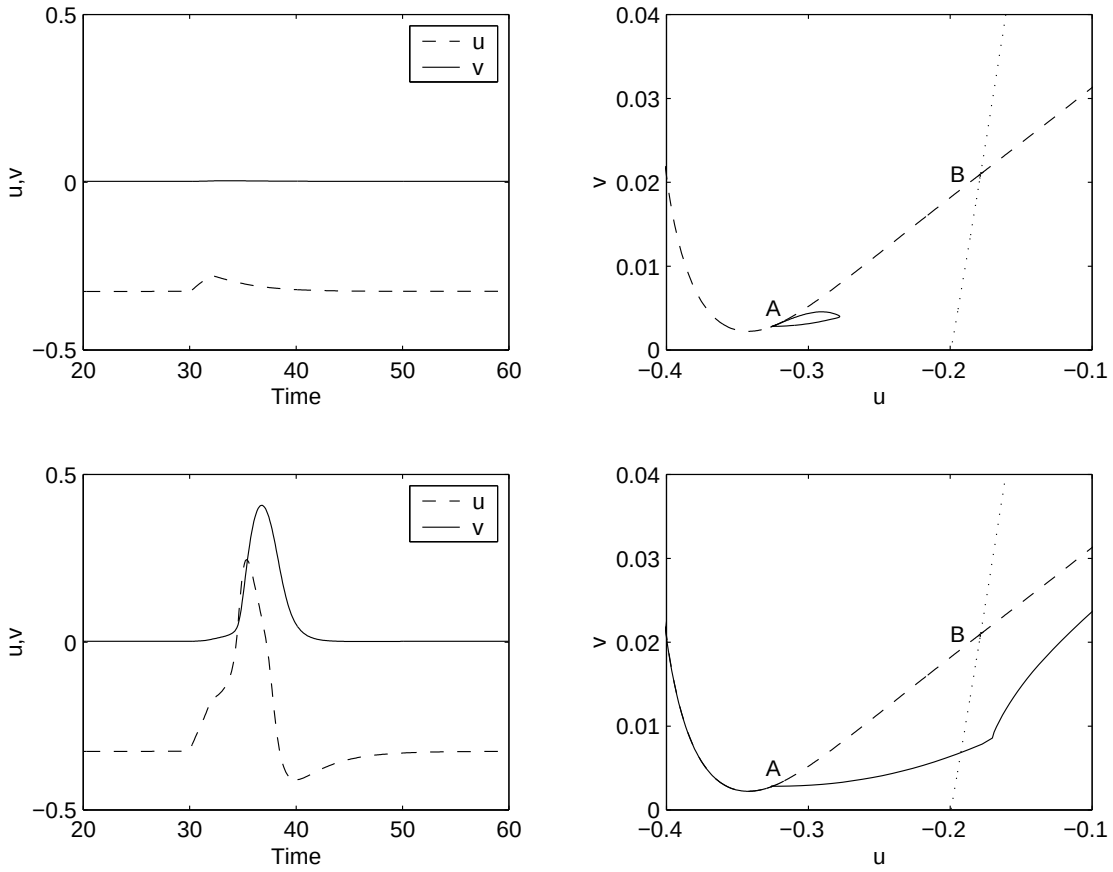

Figure 1. An example of normal excitability for the Morris–Lecar system (16)-(17). Top left: u and v as functions of time. The current was stepped from 0.07 to 0.1 during $30 < t < 32$. Top right: corresponding phase portrait. "A" is a stable node, "B" is a saddle. The unstable manifold of B is shown dashed, and the stable manifold of B is shown dotted. The trajectory is shown solid. (The right–most section of the unstable manifold of B loops up and returns to A from the left.) Bottom panels: Same as top panels, but the current was stepped from 0.07 to 0.15 for $30 < t < 32$. Note that the two fixed points A and B are annihilated in a saddle–node bifurcation at $I \approx 0.085$.

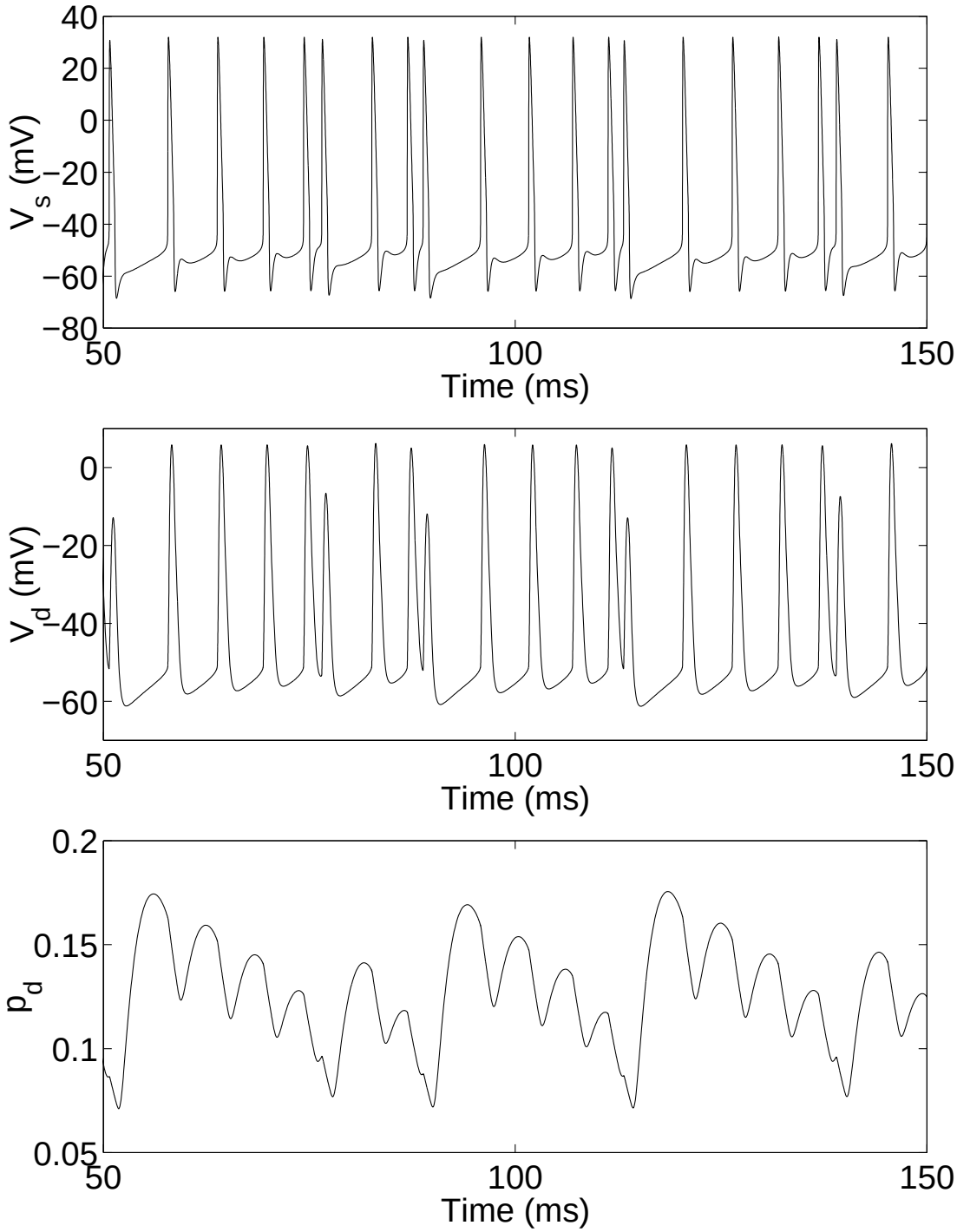

Figure 2. An example of bursting for the system (1)-(6), for $I = 10$. Top: somatic voltage. Middle: dendritic voltage. Bottom: p_d (inactivation of dendritic potassium). Bursts terminate with a high–frequency somatic "doublet" at t approximately 75, 90, 115 and 140.

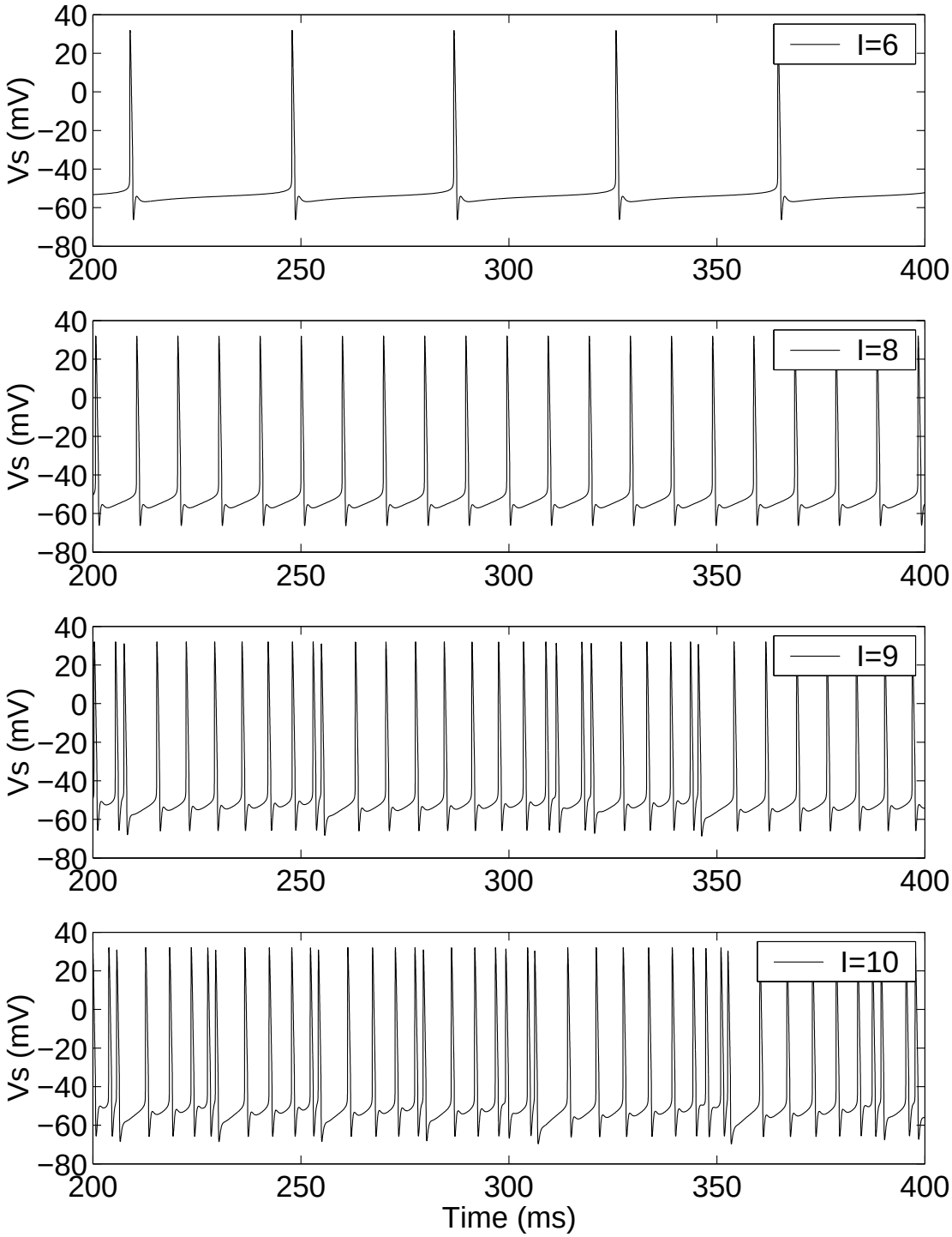

Figure 3. An example of bursting for the system (1)-(6), for $I = 6, 8, 9$ and 10 (top to bottom). The somatic voltage is plotted. In the top two panels the neuron is firing periodically, and in the bottom two it is bursting.

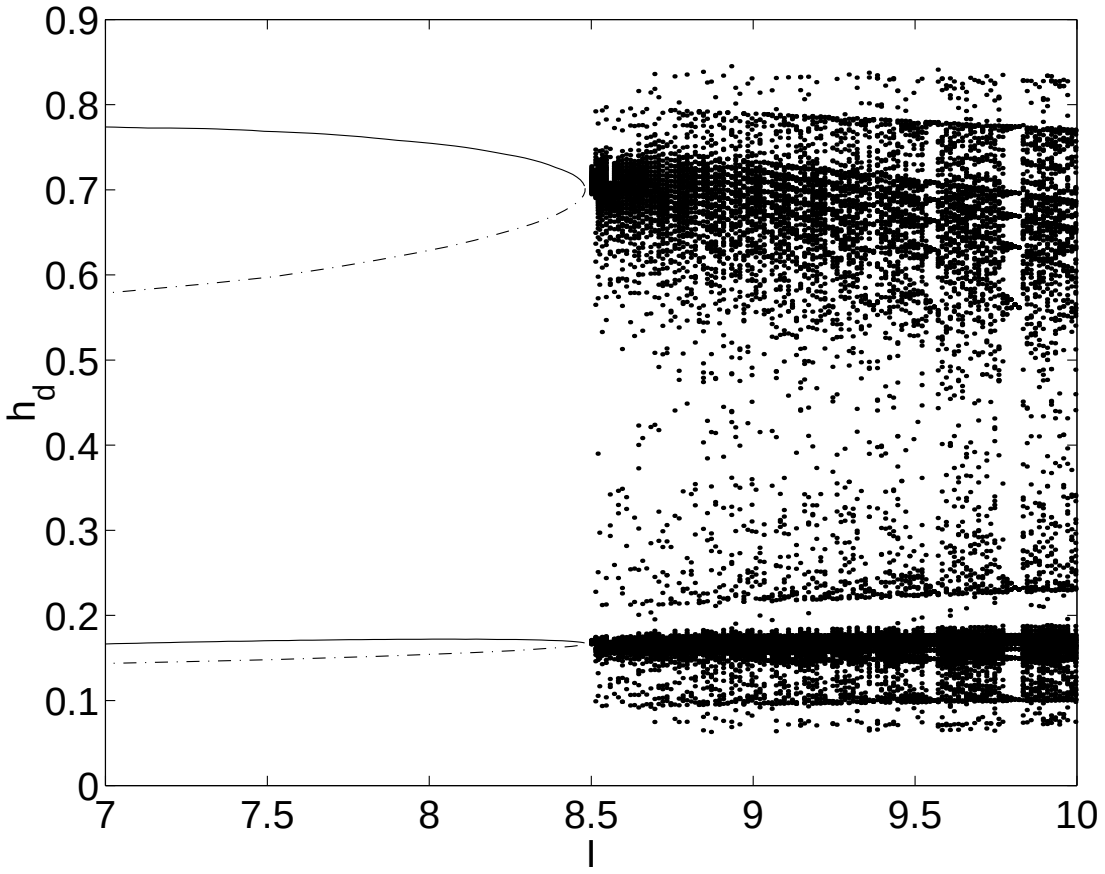

Figure 4. The bifurcation diagram for (1)-(6) as a function of I. For I less than ~ 8.5 there are two periodic orbits, one stable (solid line) and one unstable (dash–dotted). The maximum and minimum values of h_d over one period are plotted vertically. For I greater than ~ 8.5 the value of h_d at each local maximum and minimum during a period of 400 msec are plotted.

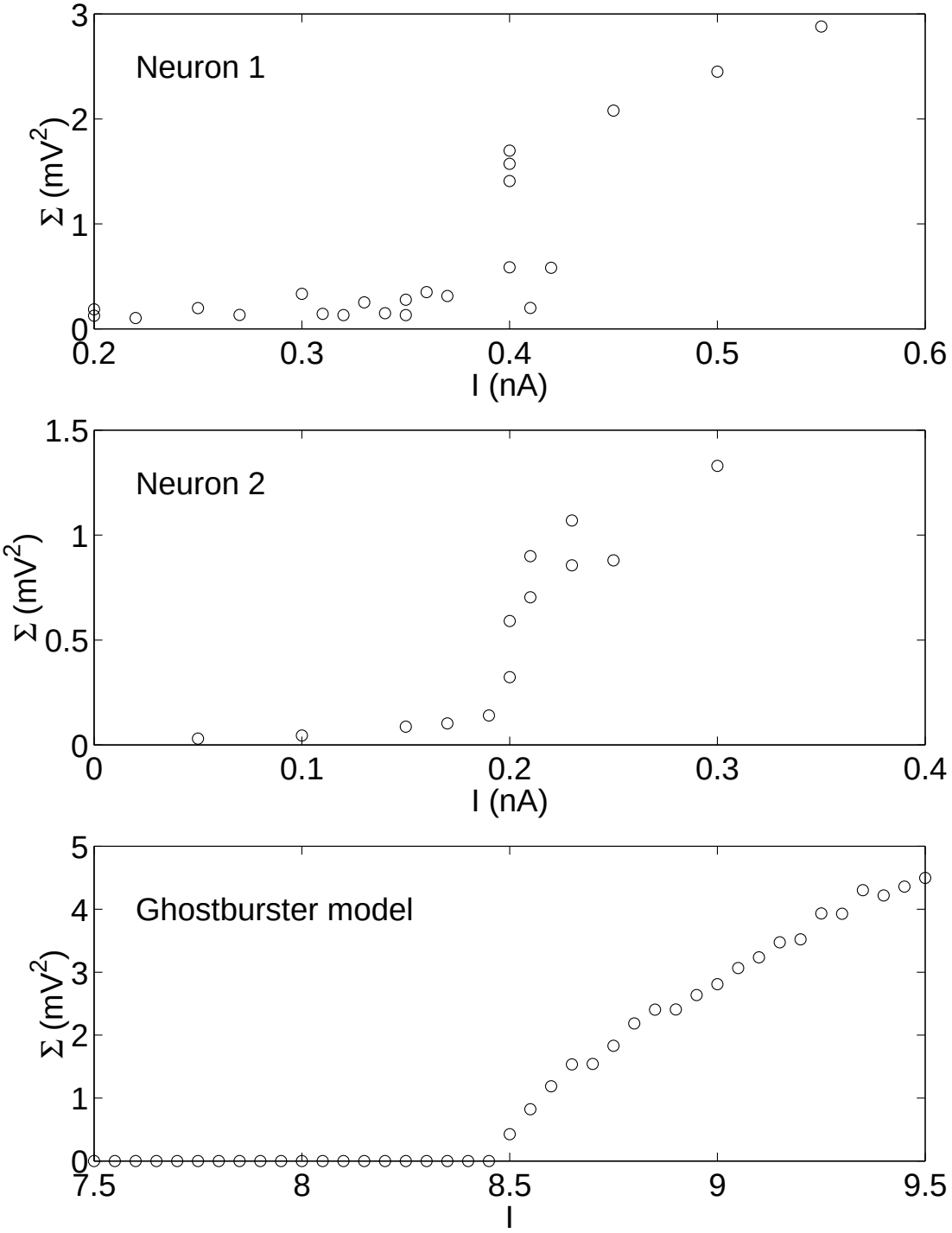

Figure 5. Top and middle: Σ, (7), as a function of somatic input current, I, for two different pyramidal cells. The number of spikes, N, was typically about 400. See Lemon and Turner (2000) for details of the methods used to record the data presented here. Bottom: Σ as a function of I for the system (1)-(6).

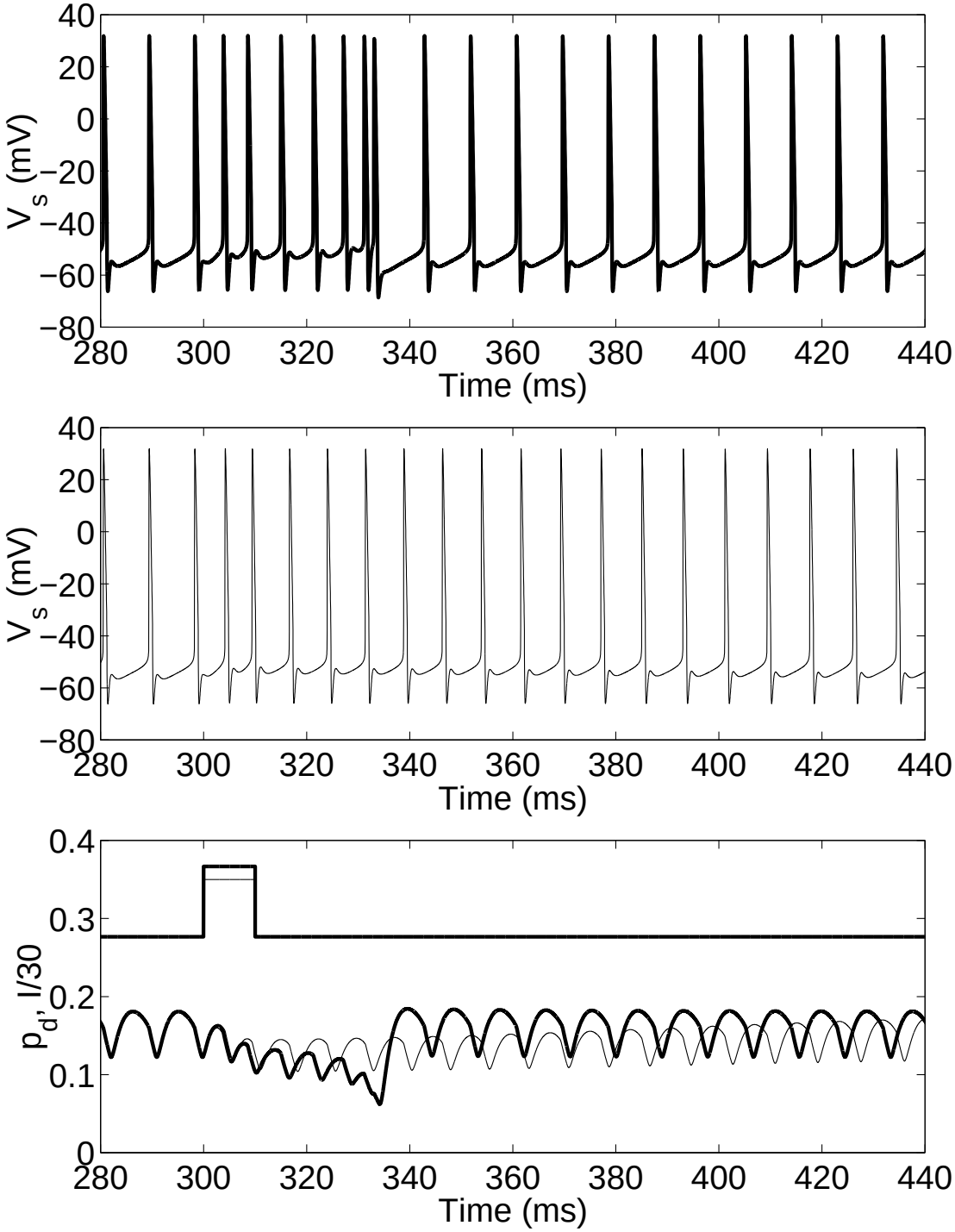

Figure 6. Burst excitability in (1)-(6). Two different current pulses (shown in the bottom panel, 1/30 their actual size) were applied. The larger one (bold line) induced a burst (top panel) that appeared about 30 ms after the stimulus, while the smaller one (thin line) did not (middle panel). Top: V_s for the large stimulus. Middle: V_s for the small stimulus. Bottom: p_d and $I/30$.

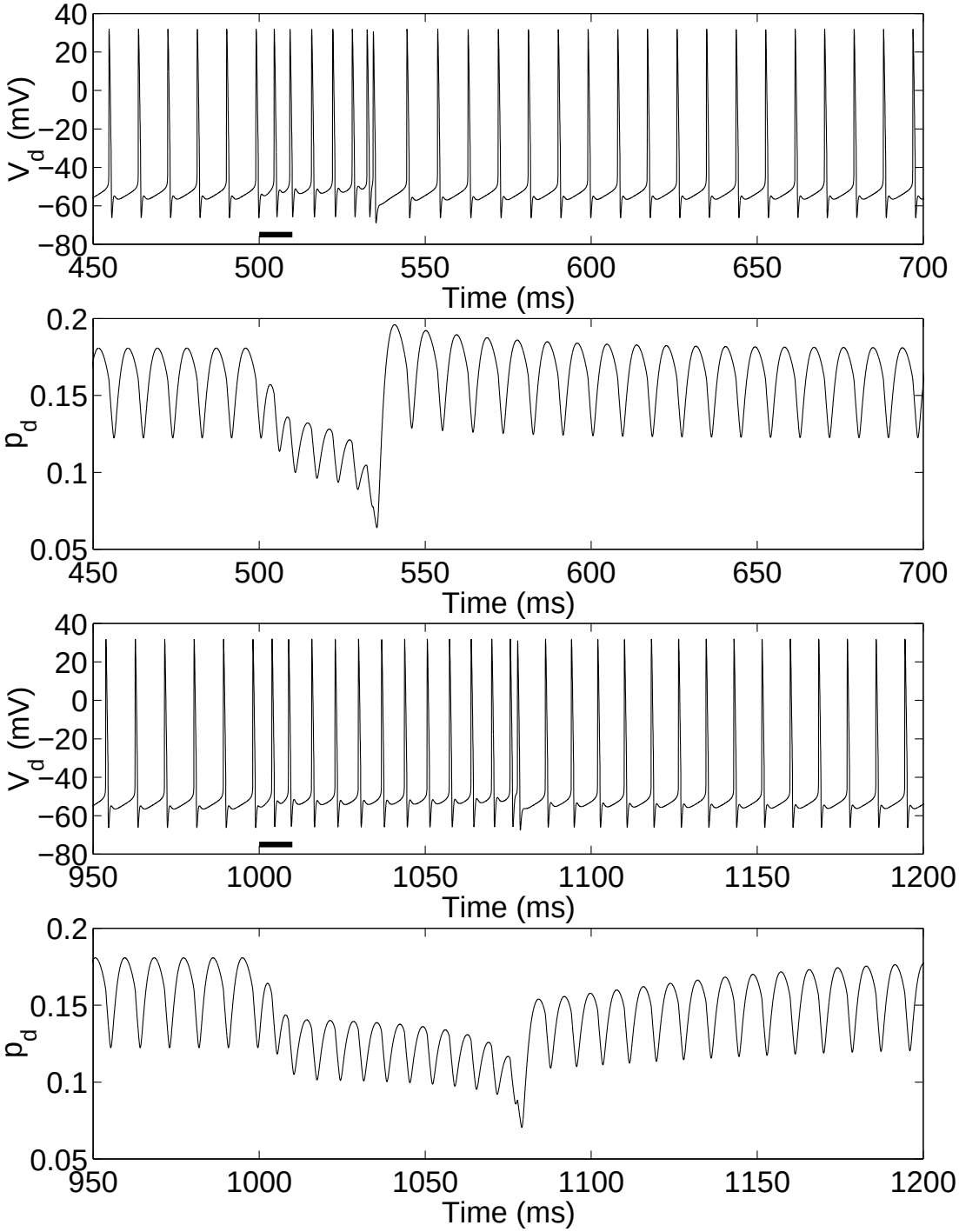

Figure 7. Different bursts induced by identical current pulses (indicated by the solid bars in the voltage panels) for the system (1)-(6). The current was stepped from 8.3 to 10.8 for 10 ms at $t = 500$ (top two panels) and again at $t = 1000$ (bottom two panels). The difference in the underlying phases at the two stimuli is approximately 1/8 of a cycle, corresponding to approximately 1 ms.

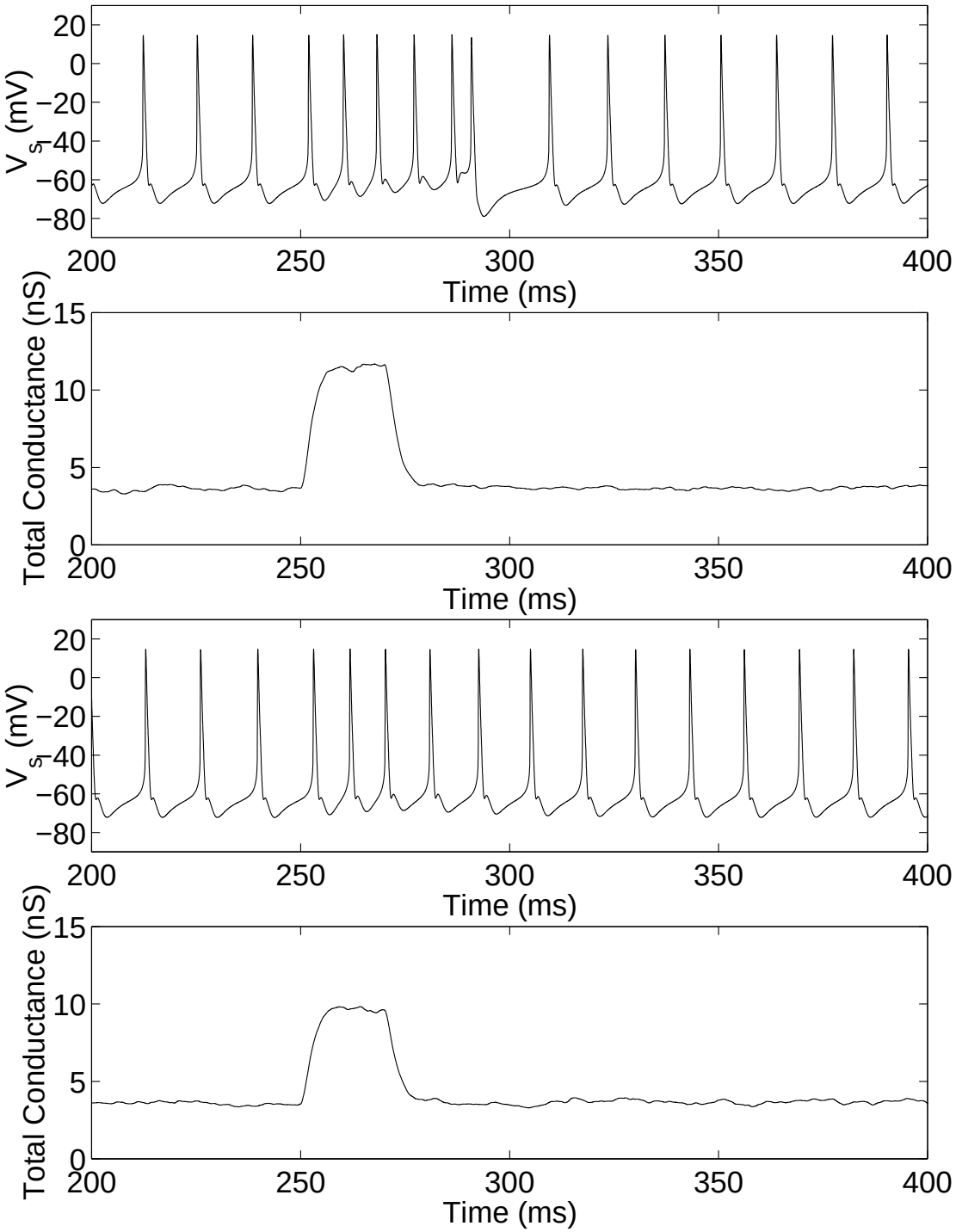

Figure 8. Burst excitability in the multicompartmental model of Doiron et al. (2001a). In the top two panels an increase in the firing rate of randomly occurring excitatory synaptic events induced a burst, whereas in the bottom two panels a slightly smaller increase in firing rate did not induce a burst. See text for details.

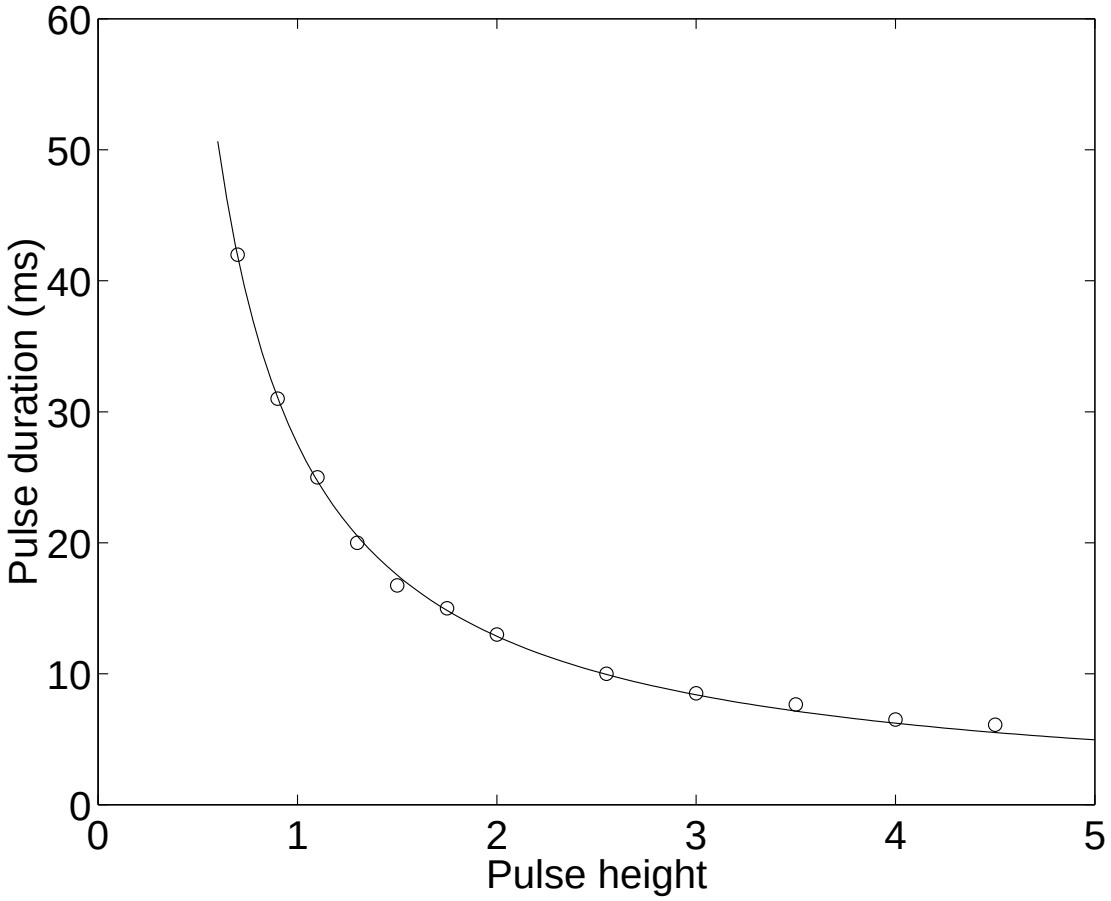

Figure 9. Minimum duration of a pulse required to generate an average of one burst per two pulses for the system (1)-(6), as a function of pulse height. Circles are numerically measured values, the solid curve is $y = 24.14/(x - 0.1235)$. The baseline current is $I = 8.3$.

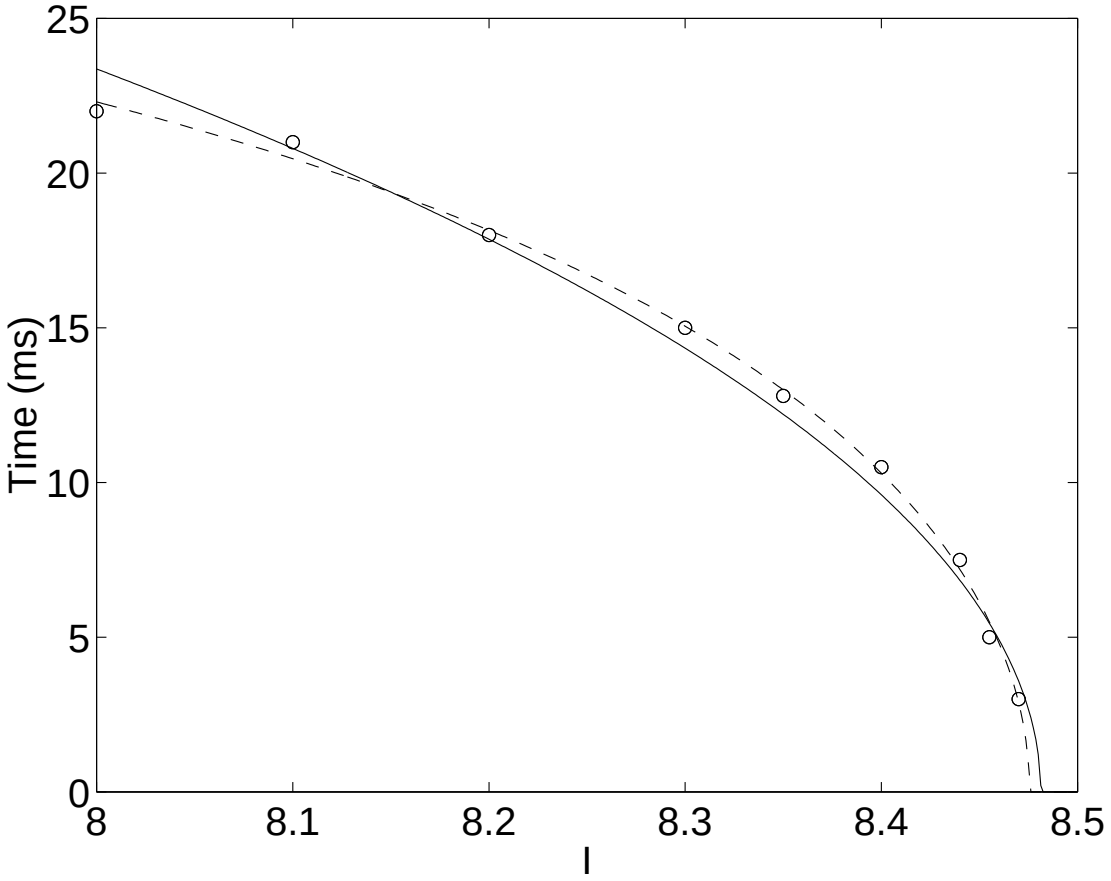

Figure 10. Minimum duration of a pulse required to generate an average of one burst per two pulses for the system (1)-(6), as a function of baseline current. $I = 10$ during a pulse. Circles are numerically measured values, the solid curve is $y = 33.69\sqrt{8.481 - x}$ and the dashed curve is $y = 32.02 \tan^{-1}\left(1.213\sqrt{8.476 - x}\right)$.

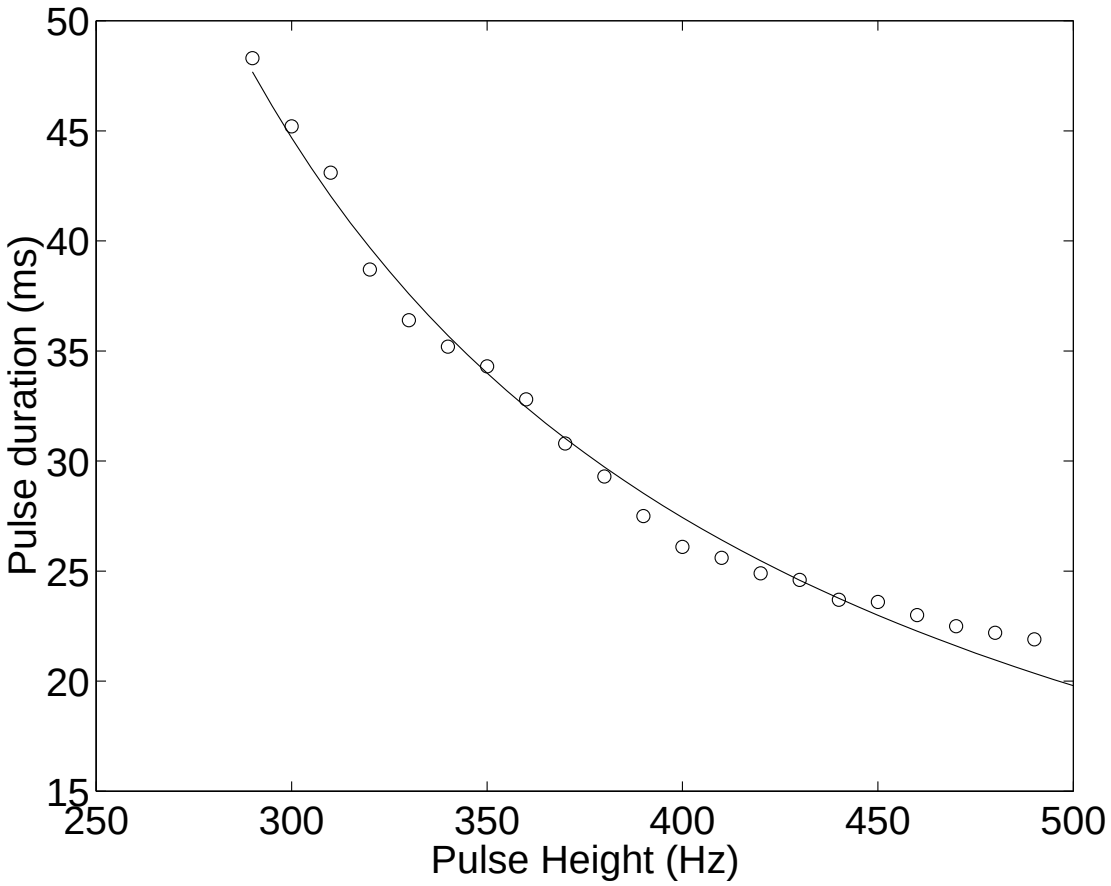

Figure 11. Minimum duration of a pulse required to generate a burst for the model described in Doiron et al. (2001a) as a function of pulse height. Circles are numerically measured values, the solid curve is the function $y = 7107/(x - 141)$. Ten noise realizations we used to obtain each data point. Compare with Figure 9.

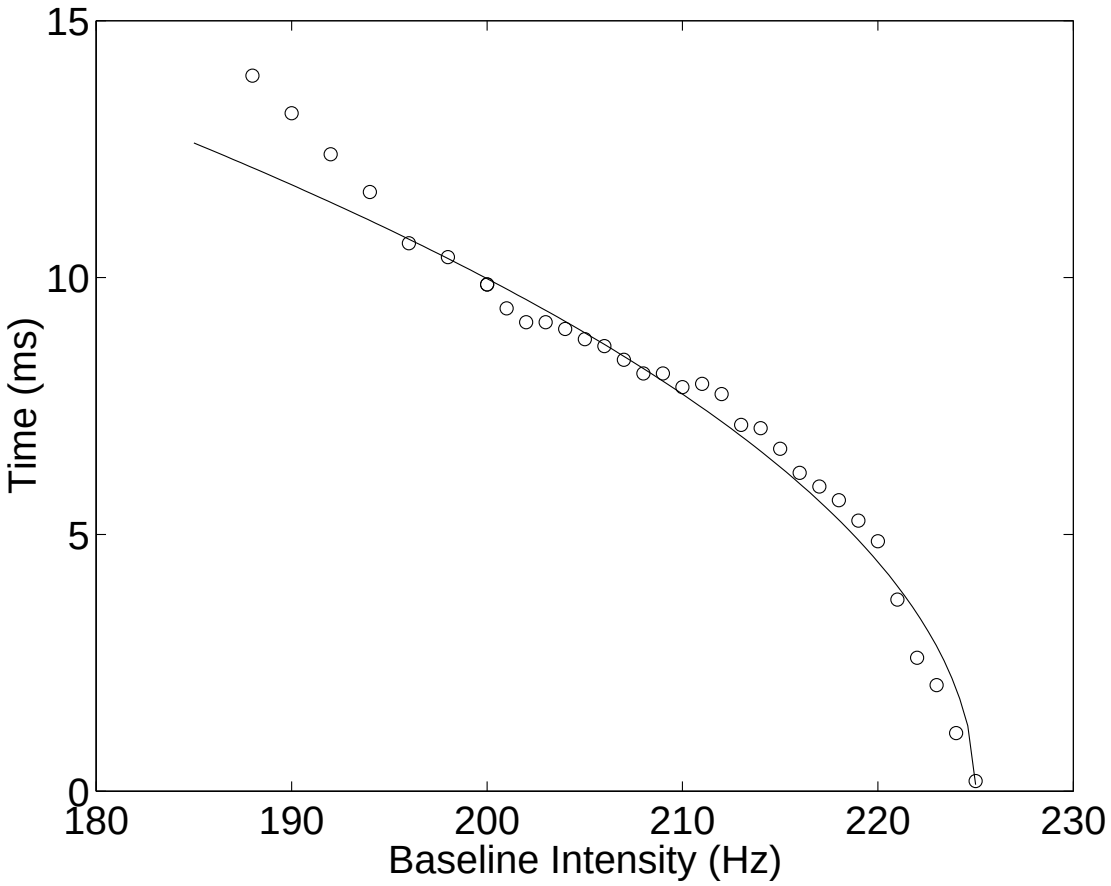

Figure 12. Minimum duration of a pulse required to generate a burst for the model described in Doiron et al. (2001a) as a function of the intensity before stimulation. Circles are numerically measured values, the solid curve is the function $y = 1.996\sqrt{225 - x}$. Ten noise realizations we used to obtain each data point. Compare with Figure 10.

Appendix

A. Equations

The Morris–Lecar system (Keener and Sneyd, 1998; Rinzel and Ermentrout, 1998) is the following pair of ODEs:

$$\frac{du}{dt} = I - g_1 m(u)(u-1) - g_K(u-u_K) - g_L(u-u_L) \tag{16}$$

$$\frac{dv}{dt} = \frac{\phi[v(u)-v]}{\tau(u)} \tag{17}$$

where

$$m(u) = \frac{1+\tanh[(u-u_1)/u_2]}{2} \tag{18}$$

$$v(u) = \frac{1+\tanh[(u-u_3)/u_4]}{2} \tag{19}$$

and

$$\tau(u) = \frac{1}{\cosh[(u-u_3)/(2u_4)]} \tag{20}$$

We use the following parameter values: $g_1 = 1, g_K = 2, u_K = -0.7, g_L = 0.5, u_L = -0.5$, $\phi = 1/3, u_1 = -0.01, u_2 = 0.15, u_3 = 0.1, u_4 = 0.145$.